RECyT
Year 26 / Nº 42 / 2024 / 39–47
DOI: https://doi.org/10.36995/j.recyt.2024.42.004

Fluoride removal from water using process residues from the cement, aggregate, and ceramic industries

Eliminación de flúor del agua utilizando residuos de procesos de las industrias de cemento, agregados y cerámica roja

Silvio Cesar Dal Pont[1]; Luana Milak Furmanski[1]; José Luiz Westrup[2]; Camila Gaspodini Tachinski[1]; Thuani Gesser Muller[1]; Alexandre Zaccaron[3]; Alexandre Gonçalves Dal-Bó[2, 3]; Michael Peterson[1, 3, *]

1- Laboratório de Reatores e Processos Industriais. Universidade do Extremo Sul Catarinense (UNESC). Av. Universitária 1105, CEP 88806-000 Criciúma, SC, Brazil.
2- Laboratório de Processamento Avançado de Polímeros. Universidade do Extremo Sul Catarinense (UNESC). Av. Universitária 1105, CEP 88806-000 Criciúma, SC, Brazil.
3- Programa de Pós-Graduação em Ciência e Engenharia de Materiais. Universidade do Extremo Sul Catarinense (UNESC). Av. Universitária 1105, CEP 88806-000 Criciúma, SC, Brazil.
* E-mail: michael@unesc.net

Received: 27/05/2024; Accepted: 30/08/2024

Abstract

The escalating demand for drinking water, coupled with the contamination of surface water sources, has intensified interest in harnessing groundwater for water supply. Elevated fluoride levels in groundwater, surpassing recommended limits (1.5 mgL^{-1}), pose a significant challenge, prohibiting the supply of water to the public. Various techniques exist for fluoride removal, with adsorption standing out for its versatility, simplicity, cost-effectiveness, and efficiency. This study assessed the kinetics and adsorption capacity of residues from the ceramic and cement industries, specifically process residues (PR) from red roof tiles, bricks, and cellular concrete. These materials, derived from the construction industry's waste, were chosen for their accessibility and low-cost preparation. Characterization through X-ray diffractometry, X-ray fluorescence spectroscopy, and isothermal nitrogen adsorption revealed cellular concrete PR as the most promising adsorbent due to its larger specific surface area (28.2 $m^2 g^{-1}$) compared to brick PR (12.6 $m^2 g^{-1}$), and roof tile PR (2.366 $m^2 g^{-1}$). Adsorption capacity followed the order: cellular concrete PR > brick PR > roof tile PR. Kinetics adhered to pseudo-first-order and pseudo-second-order models, while equilibrium studies aligned with Langmuir, Freundlich, and Sips models. Langmuir's Qmax values were 1.04, 0.709, and 1.66 (mg g^{-1}) for cellular concrete PR, brick PR, and roof tile PR, respectively, illustrating the correlation between adsorption capacity and specific surface area.

Keywords: Fluoride, Defluoridation, Adsorption, Waste.

Resumen

La demanda creciente de agua potable, junto con la contaminación de las fuentes de agua superficial, ha intensificado el interés en aprovechar el agua subterránea para el suministro de agua. Los niveles elevados de flúor en el agua subterránea, que superan los límites recomendados (1.5 mgL^{-1}), representan un desafío significativo, prohibiendo el suministro de agua al público. Existen varias técnicas para la eliminación de flúor, destacándose la adsorción por su versatilidad, simplicidad, rentabilidad y eficiencia. Este estudio evaluó la cinética y la capacidad de adsorción de residuos de las industrias cerámica y del cemento, específicamente residuos de proceso (RP) de tejas, ladrillos y concreto celular. Estos materiales, derivados de los desechos de la industria de la construcción, fueron elegidos por su accesibilidad y bajo costo de preparación. La caracterización mediante difractometría de rayos X, espectroscopía de fluorescencia de rayos X y adsorción de nitrógeno isoterma reveló que el RP de concreto celular es el adsorbente más prometedor debido a su mayor área superficial específica (28.2 $m^2 g^{-1}$) en comparación con el RP de ladrillo (12.6 $m^2 g^{-1}$) y el RP de teja (2.366 $m^2 g^{-1}$). La capacidad de adsorción siguió el orden: RP de concreto

celular > RP de ladrillo > RP de teja. La cinética se ajustó a los modelos de pseudo-primer orden y pseudo-segundo orden, mientras que los estudios de equilibrio se alinearon con los modelos de Langmuir, Freundlich y Sips. Los valores de Qmax de Langmuir fueron 1.04, 0.709 y 1.66 (mg g^{-1}) para el RP de concreto celular, RP de ladrillo y RP de teja, respectivamente, ilustrando la correlación entre la capacidad de adsorción y el área superficial específica.

Palabras clave: Flúor, Desfluoración, Adsorción, Residuos.

Introduction

Water is essential for the survival of humans and animals, but it can also be a vehicle for the transmission of diseases and harmful chemical elements. Therefore, minimum and maximum limits for harmful substances and microorganisms have been established [1]. In Brazil, these parameters are defined by the Ministry of Health [2],which provides drinking water standards and procedures for controlling and monitoring the quality of water for human consumption.

Fluoride is beneficial to human health, especially for preventing tooth decay, when used regularly at the recommended levels. However, beyond the safe limits, fluoride can be harmful. In particular, prolonged intake of water with fluoride concentrations above 2 mg L^{-1} can cause diseases such as dental fluorosis. In extreme cases, intake of water having fluoride concentrations greater than 8.0 mg L^{-1} can cause skeletal fluorosis, osteoporosis, liver and kidney damage, and thyroid changes [3–6]. According to the World Health Organization [7], and also Brazilian legislation [8], the maximum allowed concentration of fluoride in water for human consumption is 1.5 mg L^{-1} [1,4–6]. Fluorine is a common element that is widely distributed in the earth's crust and exists in the form of fluorides in various minerals, such as fluorite, cryolite, and fluorapatite. Traces of fluorides are present in many water bodies, and high fluoride concentrations are often found in groundwater. Considering the harmful effects caused by the excessive ingestion of fluoride, several techniques for the reduction of fluoride concentrations to levels suitable for human consumption are under study. Treatment techniques that have the potential to reduce the fluoride concentration of contaminated water are adsorption, chemical precipitation, ion exchange, reverse osmosis, and electrodialysis. Of these, the adsorption method is the most promising [3,5,9–11]. Adsorption is a phase transfer process that is used to remove substances from fluid phases (gases or liquids). When a solid sorbent is brought into contact with a solution, molecules or ions in the solution are adsorbed on the solid surfaces. The solid surfaces of sorbents are characterized by having active sites that are capable of interacting with solutes in the adjacent aqueous phase because of their specific electronic and spatial properties [12]. In recent years, the adsorption defluoridation method has become very attractive because of its simplicity, efficiency, low cost, and ease of operation [4–6,11,13], and many materials have been investigated as adsorbents (such as, activated alumina, bauxite, zirconium oxide, titanium hydroxide, granulated ceramics, and chitosan beads) [3–6,11,14].

The fluoride-laden waste can be converted into construction materials like bricks or concrete through solidification and stabilization processes that immobilize the fluoride, allowing the treated waste to be safely incorporated into building products [15,16]. Alternatively, the fluoride can be recovered from the waste through crystallization processes to produce valuable compounds like calcium fluoride (CaF_2) or sodium fluorosilicate (Na_2SiF_6), which have applications in industries like cement manufacturing [17,18]. By finding beneficial uses for the fluoride-containing waste after treatment, a circular economy approach can be achieved that minimizes waste disposal and promotes the sustainable management of fluoride contamination in water for human consumption [19].

In this study, we investigated the use of process residues (PR) from the cellular concrete and ceramic industries as adsorbents for aqueous fluoride. The PR were characterized by X-ray fluorescence (XRF) spectroscopy, X-ray diffractometry (XRD), and nitrogen adsorption isotherms analyzed using the Brunauer–Emmett–Teller (BET) method. Subsequently, adsorption kinetics and isothermal equilibrium adsorption studies were carried out to evaluate the adsorption capacities of the adsorbents.

Methodology

Adsorbent preparation

The residues were collected in industries in the Southern region of Santa Catarina State. Cellular concrete residues was collected in an cellular concrete Industry of and the brick and roof tile (referred to as "tile" hereinafter) residues were collected in industries located in cities near Criciúma. All materials originate from breakage during the production process. The cellular concrete is produced by a cure process using autoclave and the Brick and tile are processed by a common fire process used in the region.

The samples were ground in a hammer mill. The brick and tile PR samples were sorted through 40-mesh and 18-mesh sieves to obtain products with a minimum size of 0.4 mm and a maximum size of 1 mm. In contrast, the cellular concrete PR was sorted through sieves having 1.5 and 3.0 mm apertures. Then, the materials were washed with distilled water to eliminate the fines attached to the

particles and then washed in hydrochloric acid solution (0.1 mol L^{-1}) for 1 h with constant agitation. A third wash with distilled water was carried out to remove any excess hydrochloric acid. After the last wash, the materials were dried in an oven at (70 ± 1) °C for 24 h, without forced air circulation.

Adsorbent characterization

Chemical analysis of the samples was performed by XRF spectroscopy through fusion with lithium tetraborate using an S2 Ranger Bruker spectrometer. The mineralogical composition was analyzed by powder XRD using a Shimadzu XRD-6000 diffractometer and CuK_α radiation (λ = 1.5406 Å) generated at 25 kV and 25 mA. The XRD data were collected from 3° to 80° in 2θ at a rate of 2° min^{-1}. The specific surface areas of the materials were obtained by nitrogen adsorption measurements using the BET method. Nitrogen adsorption was carried out between relative pressures (P/P_0) of 0.05 and 0.30.

Adsorption kinetics

The adsorption kinetics tests were carried out using a Jar-Test equipment and 650 mL glass beakers containing aqueous fluoride (400 mL, 10 mg L^{-1}) and the adsorbent (6 g L^{-1}). The solutions were agitated at 120 rpm, generating a velocity gradient of 100 s^{-1}, at (25.0 ± 0.5) °C and pH 6.8–7.1. Samples were obtained at intervals of 10, 20, 30, 60, 120, 180, 240, and 300 min and filtered through white paper (pore size 28 µm) for analysis. The fluoride concentration was measured using the standard 4500-F-C method [20],using an ion-selective electrode (Thermo Scientific Orion 9609BNWP). The amount of fluoride adsorbed was determined from the mass balance, as shown in equation 1.

$$q_e = \frac{(C_0 - C_e) \cdot V}{m} \quad (1)$$

Here, q_e is the adsorption capacity (mg g^{-1}), C_0 and C_e are the initial concentration of the adsorbate and that at equilibrium, respectively, (mg L^{-1}), V is the volume of the solution (L), and m is the mass of the adsorbent (g).

The experimental data were fitted to the pseudo-first-order, pseudo-second-order, and general order kinetics models using the equations given below.

Pseudo-first-order: $$q_t = q_c[1 - \exp(-k_1 \cdot t)]$$

Pseudo-second-order: $$q_t = \frac{k_2 \cdot q_e^2 \cdot t}{k_2 \cdot q_e \cdot t + 1}$$

General order: $$q_t = q_e - \frac{q_e}{[k_N (q_e)^{n-1} \cdot t \cdot (n-1) + 1]^{1/1-n}}$$

Here, t is the contact time (min), q_t and q_e are the amounts of adsorbate adsorbed at time t and at equilibrium, respectively (mg g^{-1}), k_1 is the pseudo-first-order rate constant (min^{-1}), k_2 is the pseudo-second-order rate constant (g mg^{-1} min^{-1}), k_N is the general order rate constant [h^{-1} (mg g^{-1})n^{-1}], and n is the adsorption order with respect to the effective concentration of the adsorption sites available on the adsorbent surface.

Equilibrium adsorption

To construct the isotherms, experiments using initial concentrations of 2.5, 10, 15, and 20 mg L^{-1} of fluoride were used, and the adsorbent loading was 6 g L^{-1}. Experiments were carried out for contact time of 6 h at 25 °C. The Langmuir, Freundlich, and Sips absorption isotherms were fit to the experimental data because these models are frequently used in water and effluent treatment research [21].

The Langmuir, Freundlich, and Sips equations are given below.

Langmuir model: $$q_e = \frac{Q_{max}}{1 + K_L C_e}$$

Freundlich model: $$q_e = K_F \cdot C_e^{\frac{1}{n_F}}$$

Sips model: $$q_e = \frac{Q_{max}^{1/n_S}}{1 + K_S \cdot C_e^{1/n_S}}$$

Here, C_e (mg L^{-1}) is the adsorbate concentration at equilibrium, q_e (mg g^{-1}) is the concentration of the adsorbate at equilibrium, Q_{max} (mg L^{-1}) is the maximum adsorption capacity of the adsorbent, and K_L, K_F, and K_s are the adsorption equilibrium constants of the Langmuir, Freundlich, and Sips models, respectively. n_F and n_s are the non-dimensional exponents of the Freundlich and Sips adsorption equations, respectively.

Results

Adsorbent characterization

Table 1 lists the chemical compositions of the cellular concrete, brick, and tile PR obtained through XRF spectroscopy measurements.

Most of the minerals in the cellular concrete PR contain calcium and silicon, although there are some other elements present, including aluminum, magnesium, and iron. In the ceramic materials (tile and brick PRs), most minerals contain silicon, aluminum, and iron, although there are also smaller quantities of minerals containing potassium and titanium.

Table 1: Composition of cellular concrete, brick, and tile PR samples.

Mineral	Cellular concrete PR/(%)	Brick PR/(%)	Tile PR/(%)
Al_2O_3	1.5	21.0	19.0
CaO	25.2	0.1	0.3
Fe_2O_3	0.8	5.0	4.6
K_2O	0.2	2.2	1.4
MgO	1.4	0.7	0.5
MnO	<0.05	<0.05	<0.05
Na_2O	0.3	0.1	0.3
P_2O_5	<0.05	0.1	0.8
SiO_2	57.7	69.3	71.6
TiO_2	0.1	0.9	1.0
Weight loss	12.5	0.6	0.5

Fig. 1 shows the XRD patterns of the cellular concrete, brick, and tile PR samples.

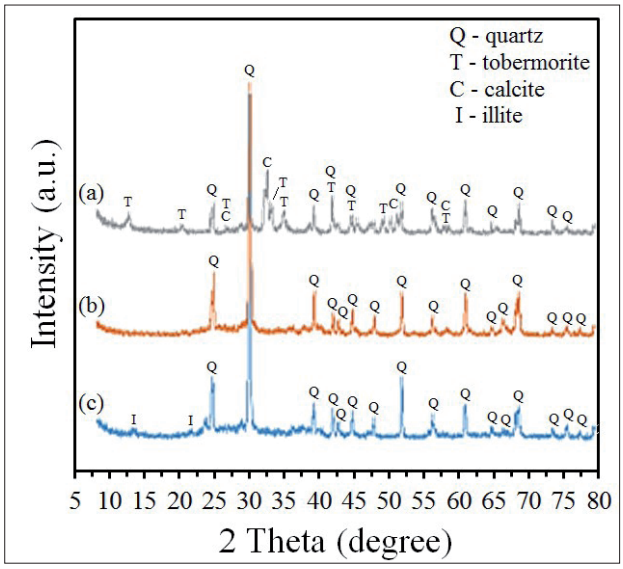

Fig. 1: Powder XRD patterns of (a) cellular concrete, (b) tile, and (c) brick PR (Q = quartz, T = tobermorite, C = calcite, and I = illite).

Analysis of the XRD pattern of the cellular concrete PR revealed the presence of to tobermorite ($Ca_5Si_6O_{16}(OH)_{24}\cdot H_2O$, JCPDS: 45-1480), quartz (SiO_2, JCPDS: 46-1045), and calcite ($CaCO_3$,JCPDS: 5-586) phases. Analysis of the XRD pattern of the brick PR revealed illite ($(K, H_2O)(Al, Mg, Fe)_2(Si, Al)_4O_{10}[(OH)_2,(H_2O)]$, JCPDS: 26-911) and quartz (SiO_2) phases. In contrast, analysis of the XRD pattern of the tile PR revealed the presence of quartz (SiO_2) alone. All of the PR samples contain quartz (SiO_2). Thus, the XRF and XRD analysis reveals that the PR samples are mixture of oxides of silicon, aluminum, iron, calcium, and magnesium. In the presence of water, these compounds can be hydrolyzed, and these species can bind fluoride to the active sites of the adsorbents [4]. The fluoride adsorption reaction can be explained by a two-step mechanism as shown in Fig. 2.

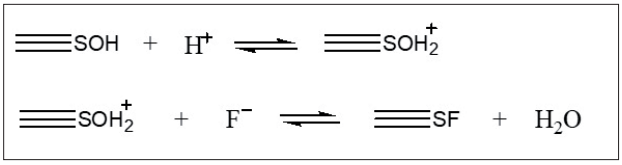

Fig. 2: Possible adsorption reactions of fluoride in aqueous media.

Table 2 lists the BET specific surface areas obtained for the cellular concrete, brick, and tile PR samples via nitrogen adsorption experiments.

Observing the results of specific surface area, it is expected that the cellular concrete PR has a greater potential for adsorption of fluorine in solution, due to the greater number of active sites [4–6].

Table 2: Specific surface area of the studied samples obtained by the BET method.

Adsorbent	Specific surface area ($m^2\ g^{-1}$)
Cellular concrete PR	28.219
Brick PR	12.621
Tile PR	2.366

Adsorption studies

Adsorption kinetics

The study of the adsorption kinetics is the first step to address the adsorbent's potential for a given separation process. Adsorption is a time-dependent process, so it is necessary to know the adsorption rate to enable the design and evaluation of an adsorbent [12]. Adsorption involves the mass transfer of the adsorbate onto the solid adsorbent and through the pores to the interior of the adsorbent. As shown in Fig. 3, fluoride was rapidly removed from solution by the cellular concrete PR. After 10 min, the removal percentage was 24.2%, and the maximum removal was 50.25% after 180 min (3 h). For the tile PR, fluoride adsorption was slow and inefficient, having a maximum removal of 7.87% after 300 min (5 h). In contrast, the removal of fluoride by the brick PR was better than that of the tile PR but worse than that of the cellular concrete PR, therefore having a middling performance, showing a slow rate of adsorption and a maximum removal of 22.13% after 300 min (5 h). These are lower than the values obtained by Yadav *et al.* [4] for brick powder (as PR brick), where between 51.0% and 56.8% of the fluoride was removed between pH 6.0 and 8.0. Possibly, the material studied by Yadav *et al*. [4] had a greater surface area, which would facilitate the adsorption of fluoride. Based on the BET specific surface areas results in Table 2, we can assume

that the specific surface areas have a strong effect on the adsorption capacity of the studied adsorbents. The cellular concrete PR has the largest specific surface areas and showed rapid adsorption in the first few minutes of the experiment because of the rapid diffusion of fluoride to the adsorbent surface, that possibly has a large number of adsorption sites [4–6,22–24]. Subsequently, adsorption slows because further adsorption requires the diffusion of the fluoride ions into the pores [4,23,25]. The brick PR, which has a surface area 55.3% smaller than that of the cellular concrete PR, removed 55.5% less fluoride than that of the cellular concrete PR. Compared to the fluoride removal of the cellular concrete PR samples, the tile PR adsorbed 84.2% less fluoride, and the tile PR has a specific surface areas 91.6% lower than that of the cellular concrete PR.

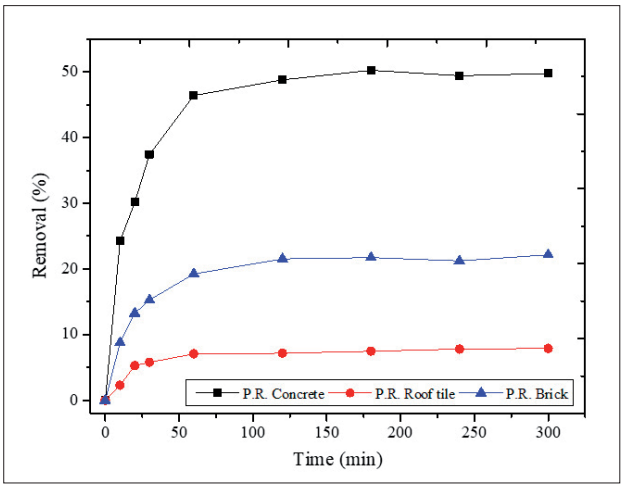

Fig. 3: Temporal evolution in fluoride adsorption by cellular concrete, tile, and brick PR adsorbents. Conditions: temperature, 25°C; adsorbent concentration, 6 g L-1; and initial fluoride concentration, 10.0 mg L-1.

The nonlinear pseudo-first-order, pseudo-second-order, and general order kinetics models (see Supplementary Information) were used to evaluate the fluoride adsorption kinetics of the adsorbents (Fig. 4 and Table 3). The initial fluoride concentration was 10.0 mg L^{-1}. After fitting, we found that only the pseudo-first-order and pseudo-second-order kinetic models fit the experimental data for all studied adsorbents.

Table 3: Kinetic parameters after fitting the kinetic models to the experimental fluoride adsorption data (initial fluoride concentration of 10.0 mg L^{-1}) for cellular concrete, tile, and brick PR samples

Kinetic parameters	Cellular concrete PR	Tile PR	Brick PR
Pseudo-first-order model			
k_f (h^{-1})	3.148	2.91	2.73
q_e(mg g^{-1})	0.823	0.127	0.359
h_0(mg g^{-1} h^{-1})*	2.59	0.369	0.982
R^2	0.988	0.981	0.993
$R^2_{adjusted}$	0.986	0.979	0.992
x^2	0.00106	0.0000380	0.000117
erf	0.0325	0.00617	0.0108
Pseudo-second-order model			
k_s(g $mg^{-1}h^{-1}$)	5.34	28.0	9.77
q_e (mg g^{-1})	0.888	0.140	0.393
h_0(mg g^{-1} h^{-1})*	4.21	0.545	1.51
R^2	0.992	0.967	0.995
$R^2_{adjusted}$	0.991	0.962	0.995
x^2	0.000670	0.0000686	0.0000720
erf	0.0259	0.00828	0.00848
General order model			
k_s(g $mg^{-1}h^{-1}$)	4.41	-	-
q_e (mg g^{-1})	0.848	-	-
h_0(mg g^{-1} h^{-1})*	3.43	-	-
R^2	0.993	-	-
$R^2_{adjusted}$	0.990	-	-
x^2	0.000631	-	-
erf	0.0251	-	-

*h_0 = Initial Adsorption Rate.

To analyze the fit of the mathematical models to the experimental data, the chi-squared (x^2) test, error function (*erf*), and coefficient of determination (R^2 and R^2_{ajd}) were used [23,26]. The kinetic parameters obtained after fitting the experimental data presented in Fig. 4 are listed in Table 3. As shown in this table, the correlation parameters R^2, R^2_{ajd}, presented higher values and the error parameters x^2 and *erf* were lowest for the pseudo-second-order and general order models for the adsorption data obtained for concrete PR. The pseudo-second-order model describes the occupation of the most active sites in the adsorption process. Thus, the adsorption rate is dependent on the

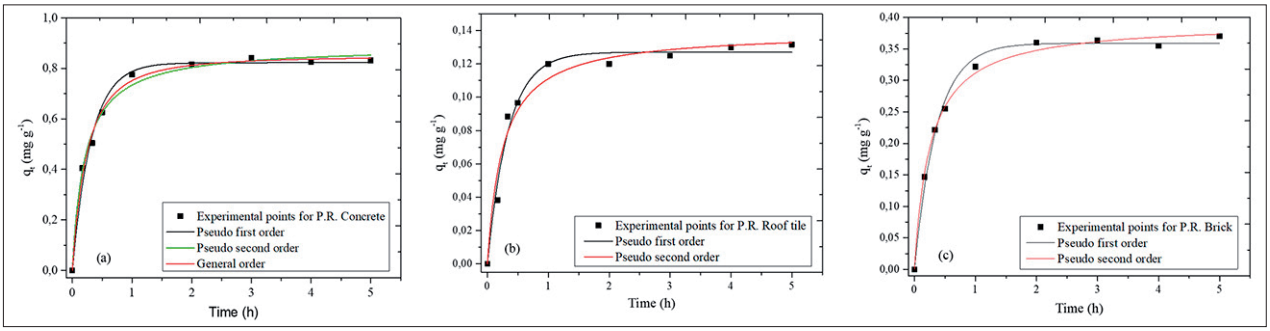

Fig. 4: Kinetics of fluoride adsorption by cellular concrete, tile, and brick PR adsorbents. Conditions: temperature 25°C; adsorbent concentration, 6 g L^{-1}; and initial fluoride concentration, 10.0 mg L^{-1}.

amount of chemical species adsorbed on the surface of the adsorbent and the amount adsorbed in the steady state [6,23,26,27]. Furthermore, the chemical adsorption process (electron sharing and exchange) is described better by this model. Therefore, the results indicate that chemisorption contributed to fluoride adsorption by the cellular concrete PR [6,23,24,27]. In the general-order kinetic model, the adsorption rate-determining step is controlled by adsorption at the adsorbent surface. In this case, during the adsorption process, both the concentration of the adsorbate in the solution and the change in the effective number of active sites at the adsorbent surface affect the adsorption kinetics [6,23,28]. For the tile PR, the pseudo-first-order model provided the best fit for the results, producing the highest correlation values of R^2, R^2_{ajd} and the lowest error values of, x^2, and *erf*. The pseudo-first-order kinetic model describes a low occupation of active sites in which the adsorption kinetics are controlled mainly by external diffusion and independent of adsorbate concentration [23,29]. The experimental data for fluoride adsorption by the brick PR fitted the pseudo-second-order model best.

Adsorption equilibrium

Adsorption equilibrium can be understood by fitting experimental adsorption data to an adsorption isotherm, thus yielding information about the adsorption process [30]. In this work, the Langmuir, Freundlich [31], and Sips isotherms were evaluated (Fig. 5 and Table 4). Based on the fitting parameters, the Freundlich model showed the best fit to the adsorption data for cellular concrete PR (Fig. 5a): the R^2_{adj}, x^2, and *erf* values are 0.984, 0.000680, and 0.0261, respectively. The low values of x^2 and *erf* indicate that the theoretical q_e is close to that measured experimentally. The Freundlich model describes the relationship between the number of species adsorbed on the sorbent and the number of species remaining in solution [30]. In this model, the active sites are not equivalent, and the adsorbate can be adsorbed in multiple layers before a monolayer is formed. In the Freundlich model, the equilibrium adsorption capacity increases with increase in the initial concentration of the adsorbate [32,33]. For the tile PR, the lowest x^2, and *erf* parameters were obtained for the Langmuir model, and this yielded a maximum adsorption capacity (Q_{max}) of 1.66 mg g^{-1}. The Langmuir model indicates the existence of a defined number of adsorption sites having equivalent energies; in addition, the adsorbed molecules do not interact with each other. Thus, adsorption occurs in a monolayer, and each site can contain only one adsorbed molecule [3,11,24,32,34]. For the brick PR, the Sips isotherm model was the best fit and yielded a Q_{max} of 0.444 mg g^{-1}. The Sips model combines the Langmuir and Freundlich isotherms and considers localized adsorption without interactions between the adsorbate species [32,35–37]. The Sips model also assumes the monolayer adsorption characteristic of the Langmuir model [32,35,37].

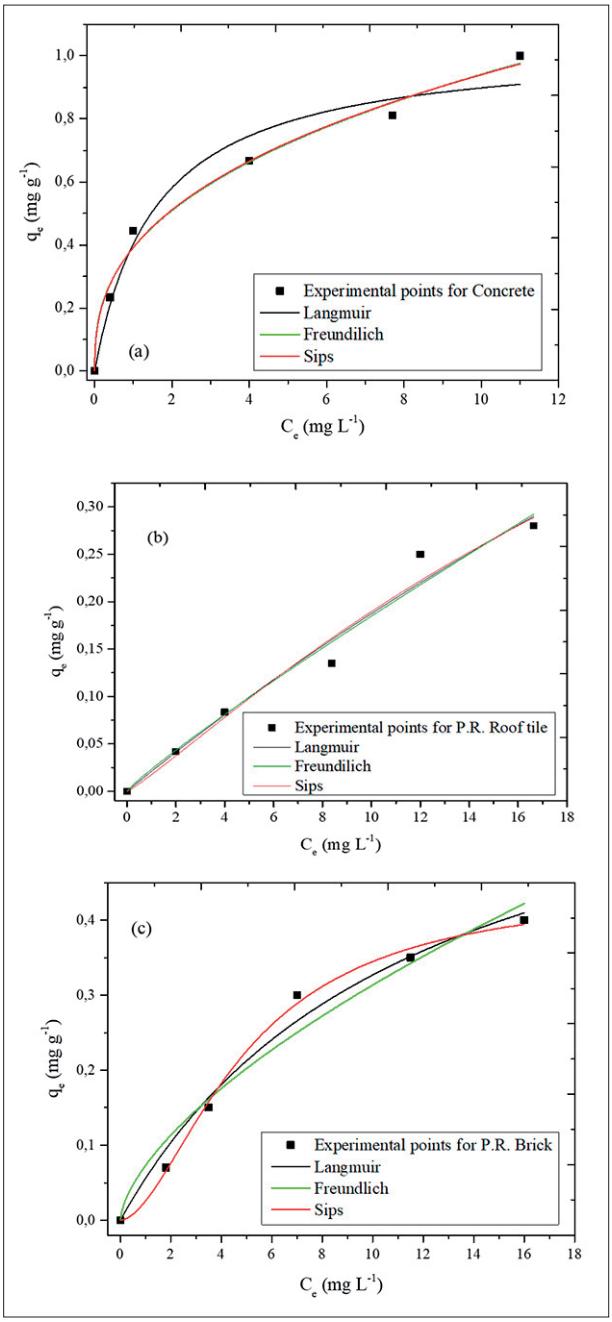

Fig. 5: Fluoride adsorption isotherms for (a–c) cellular concrete, tile, and brick PR samples, respectively. Conditions: temperature, 25°C; contact time, 6 h; and initial fluoride concentration, 2.5–20 mg L^{-1}.

Table 4: Equilibrium parameters for fluoride removal using cellular concrete, tile, and brick PR samples.

Equilibrium parameters	Cellular concrete PR	Tile PR	Brick PR
Langmuir			
Q_{max} (mg g^{-1})	1.04	1.66	0.709
K_L (L mg^{-1})	0.634	0.0128	0.0857
R^2	0.965	0.968	0.980
$R^2_{adjusted}$	0.956	0.956	0.975
x^2	0.00195	0.000160	0.000210
erf (mg g^{-1})	0.0441	0.0128	0.0144
Freundlich			
K_F (mg g^{-1}(mg $L^{-1})^{-1/n_F}$)	0.916	0.0232	0.0731
n_F	2.63	1.11	1.58
R^2	0.988	0.966	0.958
$R^2_{adjusted}$	0.984	0.958	0.947
x^2	0.000680	0.000170	0.000440
erf (mg g^{-1})	0.0261	0.0130	0.0210
Sips			
Q_{max} (mg g^{-1})	18.8	0.872	0.444
K_S (L mg^{-1})	0.0213	0.0204	0.0615
n_S	2.54	0.881	0.571
R^2	0.984	0.958	0.995
$R^2_{adjusted}$	0.972	0.930	0.992
x^2	0.000760	0.000180	0.0000440
erf (mg g^{-1})	0.0275	0.0133	0.00663

Conclusions

Among the studied adsorbents, the cellular concrete PR showed the greatest adsorption capacity and rate for the removal of fluoride from aqueous solution. Therefore, due to its efficiency, low cost and reuse of waste, enabling a reduction in the environmental impact, it makes PR cellular concrete a promising adsorbent. However, the tile and brick PR have low adsorption capacities possibly because of the low specific surface areas. Possibly, heat treatments of the adsorbents can increase the specific surface area and, consequently, the adsorption capacity. Because it is a surface phenomenon, adsorption is strongly related to the specific surface area of the material, as shown by the adsorption capacities and specific surface areas, which both decrease in order of cellular concrete PR >brick PR >tile PR. Analysis of the adsorption kinetics revealed that the cellular concrete and brick PR mainly adsorbed fluoride via chemisorption, whereas the tile PR mainly adsorbed fluoride by physisorption. Modeling of the adsorption process revealed that the cellular concrete, tile, and brick PR adsorbents best fit the Freundlich, Langmuir, and Sips isotherms, respectively, indicating that the brick and tile PR samples adsorb fluoride in a monolayer, whereas the cellular concrete PR adsorbs fluoride by multilayer adsorption.

Acknowledgements: This study was supported by the Coordenação de Aperfeiçoamento de Pessoal de Nível Superior (CAPES/Brazil) and the Fundação de Amparo à Pesquisa e Inovação ao do Estado de Santa Catarina (FAPESC/Brazil).

Author Contributions: S.C.D.P.: conceptualization, data curation, writing original draft; L.M.F.: investigation; J.L.W.: formal analysis, validation; C.G.T.: formal analysis; T.G.M.: formal analysis; A.Z.: writing-review & editing, visualization; A.G.D.B.: funding acquisition, resources; M.P.: project administration, resources, validation.

Conflicts of interest: The authors declare that they have no known competing financial interests or personal relationships that could have appeared to influence the work reported in this paper.

References

1. **Dhar, V.; Bhatnagar, M.** *Physiology and Toxicity of Fluoride.* Indian J. Dent. Res. 2009, 20, 350, doi:10.4103/0970-9290.57379.
2. **Brazil Portaria de Consolidação No. 5.** *Consolidação das normas sobre as ações e os serviços de saúde do sistema único de saúde.*
3. **He, Y.; Zhang, L.; An, X.; Wan, G.; Zhu, W.; Luo, Y.** *Enhanced Fluoride Removal from Water by Rare Earth (La and Ce) Modified Alumina: Adsorption Isotherms, Kinetics, Thermodynamics and Mechanism.* Sci. Total Environ. 2019, 688, 184–198, doi:10.1016/j.scitotenv.2019.06.175.
4. **Yadav, A.; Kaushik, C.; Haritash, A.; Kansal, A.; Rani, N.** *Defluoridation of Groundwater Using Brick Powder as an Adsorbent.* J. Hazard. Mater. 2006, 128, 289–293, doi:10.1016/j.jhazmat.2005.08.006.
5. **Lee, J.-I.; Kang, J.-K.; Hong, S.-H.; Lee, C.-G.; Jeong, S.; Park, S.-J.** *Thermally Treated Mytilus Coruscus Shells for Fluoride Removal and Their Adsorption Mechanism.* Chemosphere 2021, 263, 128328, doi:10.1016/j.chemosphere.2020.128328.
6. **Lee, G.; Chen, C.; Yang, S.-T.; Ahn, W.-S.** *Enhanced Adsorptive Removal of Fluoride Using Mesoporous Alumina.* Microporous Mesoporous Mater. 2010, 127, 152–156, doi:10.1016/j.micromeso.2009.07.007.
7. **Organization, W.H.** *Guidelines for Drinking-Water Quality Recommendation.* World Health Organization. Geneva, Switz. 2004.
8. **BRASIL Portaria N° 518, de 25 de Março de 2004.** *Legislaçã Para Águas de Consumo Humano*; Brasilia, DF, 2004;
9. **Onyango, M.S., Matsuda, H.** *Chapter 1.* Fluoride Removal from Water Using Adsorption Technique. In Advances in Fluorine Science; 2006; pp. 1–48.
10. **Bhatnagar, A.; Kumar, E.; Sillanpää, M.** *Fluoride Removal from Water by Adsorption—A Review.* Chem. Eng. J. 2011, 171, 811–840, doi:10.1016/j.cej.2011.05.028.
11. **Borgohain, X.; Boruah, A.; Sarma, G.K.; Rashid, M.H.** *Rapid and Extremely High Adsorption Performance of Porous MgO Nanostructures for Fluoride Removal from*

Water. J. Mol. Liq. 2020, 305, 112799, doi:10.1016/j.molliq.2020.112799.

12. **Oguz, E.** *Equilibrium Isotherms and Kinetics Studies for the Sorption of Fluoride on Light Weight Concrete Materials.* Colloids Surfaces A Physicochem. Eng. Asp. 2007, 295, 258–263, doi:10.1016/j.colsurfa.2006.09.009.
13. **Gao, S.; Cui, J.; Wei, Z.** *Study on the Fluoride Adsorption of Various Apatite Materials in Aqueous Solution.* J. Fluor. Chem. 2009, 130, 1035–1041, doi:10.1016/j.jfluchem.2009.09.004.
14. **Masquetti da Conceição, V.; Bassetti, F.D.J.; Bergamasco, R.** *Desfluoretação de Águas Subterrâneas a Partir Da Coagulação/Floculação Com Coagulante Natural de Semente de Moringa Oleifera Lam.* e-xacta 2013, 6, 121, doi:10.18674/exacta.v6i2.1005.
15. **Olejarczyk, M.; Rykowska, I.; Urbaniak, W.** *Management of Solid Waste Containing Fluoride—A Review.* Materials (Basel). 2022, 15, 3461, doi:10.3390/ma15103461.
16. **Ismail, Z.Z.; AbdelKareem, H.N.** *Sustainable Approach for Recycling Waste Lamb and Chicken Bones for Fluoride Removal from Water Followed by Reusing Fluoride-Bearing Waste in Concrete.* Waste Manag. 2015, 45, 66–75, doi:10.1016/j.wasman.2015.06.039.
17. **Zueva, S.; Ferella, F.; Corradini, V.; Baturina, E. V.; Ippolito, N.M.; Vegliò, F.** *An Effective New Treatment of Fluoride-Containing Sludge Resulting from the Manufacture of Photovoltaic Cells.* Processes 2021, 9, 1745, doi:10.3390/pr9101745.
18. **Lacson, C.F.Z.; Lu, M.-C.; Huang, Y.-H.** *Fluoride-Rich Wastewater Treatment by Ballast-Assisted Precipitation with the Selection of Precipitants and Discarded or Recovered Materials as Ballast.* J. Environ. Chem. Eng. 2021, 9, 105713, doi:10.1016/j.jece.2021.105713.
19. **Amini, M.; Mueller, K.; Abbaspour, K.C.; Rosenberg, T.; Afyuni, M.; Møller, K.N.; Sarr, M.; Johnson, C.A.** *Statistical Modeling of Global Geogenic Fluoride Contamination in Groundwaters.* Environ. Sci. Technol. 2008, 42, 3662–3668, doi:10.1021/es071958y.
20. **Rice, E.W., Baird, R.B., Eaton, A.D., Clesceri, L.S.** *American Public Health Association, American Water Works Association, Water Environment Federation: Standard Methods for Examination of Water and Wastewater (22nd Edition).* Am. Public Heal. Assoc. 2012.
21. **Azizian, S.** *Kinetic Models of Sorption: A Theoretical Analysis.* J. Colloid Interface Sci. 2004, 276, 47–52, doi:10.1016/j.jcis.2004.03.048.
22. **Liu, H.; Dong, Y.; Wang, H.; Liu, Y.** *Adsorption Behavior of Ammonium by a Bioadsorbent – Boston Ivy Leaf Powder.* J. Environ. Sci. 2010, 22, 1513–1518, doi:10.1016/S1001-0742(09)60282-5.
23. **Westrup, J.L.; Bertoldi, C.; Cercena, R.; Dal-Bó, A.G.; Soares, R.M.D.; Fernandes, A.N.** *Adsorption of Endocrine Disrupting Compounds from Aqueous Solution in Poly(Butyleneadipate-Co-Terephthalate) Electrospun Microfibers.* Colloids Surfaces A Physicochem. Eng. Asp. 2021, 611, 125800, doi:10.1016/j.colsurfa.2020.125800.
24. **Yang, K.; Li, Y.; Tian, Z.; Peng, K.; Lai, Y.** *Removal of Fluoride Ions from ZnSO4 Electrolyte by Amorphous Porous Al2O3 Microfiber Clusters: Adsorption Performance and Mechanism.* Hydrometallurgy 2020, 197, 105455, doi:10.1016/j.hydromet.2020.105455.
25. **Prola, L.D.T.; Acayanka, E.; Lima, E.C.; Umpierres, C.S.; Vaghetti, J.C.P.; Santos, W.O.; Laminsi, S.; Djifon, P.T.** *Comparison of Jatropha Curcas Shells in Natural Form and Treated by Non-Thermal Plasma as Biosorbents for Removal of Reactive Red 120 Textile Dye from Aqueous Solution.* Ind. Crops Prod. 2013, 46, 328–340, doi:10.1016/j.indcrop.2013.02.018.
26. **Guo, X.; Wang, J. A** *General Kinetic Model for Adsorption: Theoretical Analysis and Modeling.* J. Mol. Liq. 2019, 288, 111100, doi:10.1016/j.molliq.2019.111100.
27. **Ho, Y.S.; McKay, G.** *Sorption of Dye from Aqueous Solution by Peat.* Chem. Eng. J. 1998, 70, 115–124, doi:10.1016/S0923-0467(98)00076-1.
28. **Shawabkeh, R.** *Experimental Study and Modeling of Basic Dye Sorption by Diatomaceous Clay.* Appl. Clay Sci. 2003, 24, 111–120, doi:10.1016/S0169-1317(03)00154-6.
29. **Malik, P.K.** *Use of Activated Carbons Prepared from Sawdust and Rice-Husk for Adsorption of Acid Dyes: A Case Study of Acid Yellow 36.* Dye. Pigment. 2003, 56, 239–249, doi:10.1016/S0143-7208(02)00159-6.
30. **Ribas, M.C.; Adebayo, M.A.; Prola, L.D.T.; Lima, E.C.; Cataluña, R.; Feris, L.A.; Puchana-Rosero, M.J.; Machado, F.M.; Pavan, F.A.; Calvete, T.** *Comparison of a Homemade Cocoa Shell Activated Carbon with Commercial Activated Carbon for the Removal of Reactive Violet 5 Dye from Aqueous Solutions.* Chem. Eng. J. 2014, 248, 315–326, doi:10.1016/j.cej.2014.03.054.
31. **Freundlich, H.** *Über Die Adsorption in Lösungen.* Zeitschrift für Phys. Chemie 1907, 57U, doi:10.1515/zpch-1907-5723.
32. **Rovani, S.; Censi, M.T.; Pedrotti, S.L.; Lima, É.C.; Cataluña, R.; Fernandes, A.N.** *Development of a New Adsorbent from Agro-Industrial Waste and Its Potential Use in Endocrine Disruptor Compound Removal.* J. Hazard. Mater. 2014, 271, 311–320, doi:10.1016/j.jhazmat.2014.02.004.
33. 33. **Fujiwara, I.; Suzuki, K.; Shin, S.; Sato, M.** *Adsorption Properties of High-Silica Zeolites for High-Temperature Chemical Heat Pumps.* J. Chem. Eng. Japan 1990, 23, 738–744, doi:10.1252/jcej.23.738.
34. **Guan, C.; Lv, X.; Han, Z.; Chen, C.; Xu, Z.; Liu, Q.** *The Adsorption Enhancement of Graphene for Fluorine and Chlorine from Water.* Appl. Surf. Sci. 2020, 516, 146157, doi:10.1016/j.apsusc.2020.146157.
35. **Lima, É.C., Adebayo, M.A., Machado, F.M.**. *Kinetic and Equilibrium Models of Adsorption.* Carbon Nanostructures

2015, 33–69.

36. **Sips, R.** *On the Structure of a Catalyst Surface.* J. Chem. Phys. 1948, 16, 490–495, doi:10.1063/1.1746922.

37. **Kumara, N.T.R.N.; Hamdan, N.; Petra, M.I.; Tennakoon, K.U.; Ekanayake, P.** *Equilibrium Isotherm Studies of Adsorption of Pigments Extracted from Kuduk-Kuduk (Melastoma Malabathricum L.) Pulp onto TiO 2 Nanoparticles.* J. Chem. 2014, 2014, 1–6, doi:10.1155/2014/468975.